High Contrast Ultrasound Images of Defects in Food Package Seals

Catherine H. Frazier, *Student Member, IEEE*, Qi Tian, *Member, IEEE*, Ayhan Ozguler, Scott A. Morris, and William D. O'Brien, Jr., *Fellow, IEEE*

***Abstract*—Previous work to detect defects in food packaging seals using pulse-echo ultrasound inspired the backscattered amplitude integral (BAI) imaging technique, which could reliably identify channels with diameters 38 μm or larger at a center frequency of 17.3 MHz ($\lambda = 86$ μm). The current study presents two new processing techniques that more reliably reveal smaller channels (≈ 6 μm in diameter). The RF sampling technique (RFS) displays a single, time-gated, pressure value from the received (not envelope-detected) RF waveform at each transducer position. The RF correlation technique (RFC) calculates the correlation coefficients of the RF signals with a reference signal that does not pass through a channel. The correlation coefficient can be calculated for the entire RF signal (RFCE) or over a short segment of the RF signal (RFCS). The performance of these imaging methods for detecting channel defects is investigated for plastic and aluminum foil trilaminate films with 6, 10, 15, 38, and 50 μm channels filled with water or air. Data are collected with a focused ultrasound transducer (17.3 MHz, 6.35 mm in diameter, f/2, 173 μm -6 dB pulse-echo lateral beamwidth at the focus) scanned over a rectangular grid, keeping the package in the focus. Performance is measured using detection rates, image contrast, and contrast-to-noise ratio (CNR). Both RFS and RFCS have improved detection rates relative to BAI for channels 15 μm or smaller. The RFCS technique is the most effective at smoothing the background, leading to the greatest CNR improvements.**

I. Introduction

An important part of the food packaging process is the detection of flaws in the package's seal. Flaws include areas where the seal has wrinkled, failed to seal, or is filled with air, water, food material, or other contaminants. Channel leaks, in particular, can cause a pathway for microbial penetration that results in spoilage of the product or in pathogen growth. Currently, detection of flaws in the seal region of flexible food packages is accomplished through visual inspection or through destructive testing. However, channels smaller than 50 μm in diameter are not clearly visible to the naked eye, and destructive testing is only valuable in a statistical sense [1]. To ensure the safety of shelf-stable food despite these poor testing methods, it is generally stored and reinspected for spoilage after storage, which increases the cost of the product and reduces production speed.

Similar problems of detecting flaws in layered material have been studied through ultrasonic nondestructive evaluation of composite materials. Frock and Martin [2] showed that defects in graphite/epoxy composites, which are small compared with the length of the transmitted pulse, were not visible in C-mode images because of surface roughness, variations in attenuation by the material, and variable thickness of the material. The defects could be more easily revealed by processing the C-mode image, using a 3×3 mask to implement edge enhancement or localized histogram modification. Kazys and Svilainis [3] detected delaminations in thin (thickness less than a wavelength) three-layer aramide-fiber-reinforced ARALL-type composites. They used a modified L1 norm deconvolution and frequency domain imaging technique. Both techniques allowed them to determine the location of the delamination. Unlike Frock and Martin's study [2], which applies post-processing to the C-mode image, our study shows new imaging techniques to improve detectability, and our techniques are intended for use on smaller defects than those studied by Kazys and Svilainis [3].

Previous investigations of food packages have shown that channels in packaging seals, which are generally smaller than defects in composite materials, can be detected using the BAI imaging technique [4]. BAI images display the integral of the envelope-detected RF signal at each transducer position over a rectangular scan area. Channels with diameters 38 μm or larger can be detected reliably using this technique at a center frequency of 17.3 MHz. However, the BAI technique is unable to detect reliably channel defects smaller than 38 μm. Improved signal processing methods are needed.

The RFS method displays, for each transducer position, a single time-gated acoustic pressure value of the received RF waveform. The processing for RFS is very simple, involving only a single time gate. Because no envelope detection is required to form the image, and no processing is required after the image has been formed, images are created very quickly, and, therefore, this new method is well-suited for production line use. For RFS to be useful, a method must be formulated for choosing the point from each waveform for display, and images created using that point must reliably show channels when they exist. The

Manuscript received March 30, 1999; accepted August 22, 1999. This work was supported by NSF Fellowship (CHF) and by the Value-Added Research Opportunities Program, Agricultural Experiment Station, University of Illinois.

C. H. Frazier, Q. Tian, and W. D. O'Brien, Jr. are with Bioacoustics Research Laboratory, Department of Electrical and Computer Engineering, University of Illinois, Urbana, IL 61801 (e-mail: wdo@uiuc.edu).

A. Ozguler and S. A. Morris are with Packaging Program, Department of Food Science and Human Nutrition, University of Illinois, Urbana, IL 61801.

selection of points requires knowledge of the thickness and average speed of sound in the packaging material, which can be obtained off-line. By selecting only one point on the received RF waveform, there is a risk that a channel is present but not detected. This risk can be reduced by forming multiple images with several time gates.

RFC requires less specific a priori information and offers potentially higher detectability at a cost of greater computational complexity. Although the exact depth of the channel defect is generally unknown, very coarse range estimation can be given. Then, a window can be placed over this range and the normalized correlation coefficient between RF signals can be calculated.

In the next section, we give a brief overview of the data collection procedure. In Section III, we discuss the appearance of channels in B-mode images that led to the consideration of new techniques. Section IV describes the image formation techniques and the analysis, including the method used for comparing the imaging methods. In Section V, we compare the three techniques in terms of channel detection rates, image contrast, and CNR. Finally, conclusions and suggestions for future work are given in Section VI.

II. Data Collection

The materials and data collection method are discussed extensively in [5]; therefore, these details will be mentioned only briefly here. Two types of packaging film are examined, each with three layers of material. The first type of film is plastic trilaminate with a layer of polypropylene (80 μm; $c = 2660$ m/s), a layer of polyvinylidene chloride (PVDC) (15 μm; $c = 2380$ m/s), and a layer of oriented nylon (15 μm; $c = 2600$ m/s). The overall film is 110 μm thick with a measured average speed of 2380 m/s. The second type of packaging film is an aluminum foil trilaminate with a layer of polypropylene ($c = 2660$ m/s), a layer of aluminum foil ($c = 6420$ m/s), and a layer of polyester ($c = 1950$ m/s). The individual material thicknesses for this material are unknown. The overall thickness of this film is 120 μm, and the measured average speed is 2460 m/s.

Smooth, die-drawn tungsten wires with 6, 10, 15, 38, and 50-μm diameters are used to prepare the channel defects. Each test object used in this study contains one defect. Defects are created by using an automatic heat sealer to fuse together two films with a tungsten wire in between and removing the wire after the seal has cooled. The water-filled channel is created by removing the wire axially with the packaging material submerged in a water bath and then sealing the ends of the channel. The air-filled channel is created similarly by removing the wire with the sample in air and then sealing the ends of the channel. For notational convenience, channel defects are classified as air-filled channel within plastic (ACP), water-filled channel within plastic (WCP), air-filled channel within aluminum foil (ACA), and water-filled channel within aluminum foil (WCA). No smaller channels were made because of complications with smaller wires. It is difficult to remove them without breaking the wire.

Defect sizes have been confirmed using a light transmission microscope. In general, the defects are somewhat elliptical in shape; however, their approximate diameters closely resemble the diameters of the wires used to create them [5]. Therefore, we refer only to the diameter of the wire when describing the channel size. Throughout this paper, channels 38 μm or larger are referred to as large or moderate-sized channels. Channels 15 μm or smaller are referred to as small channels.

A three-dimensional data set is collected using a nominal 20-MHz focused transducer (V317; Panametrics, Waltham, MA) operating with at a center frequency of 17.3 MHz (6.35 mm in diameter, f/2, 173 μm -6 dB pulse-echo lateral beamwidth at the focus). The transducer is shock-excited by a pulser-receiver (Model 5800; Panametrics) with a 300 V monocycle pulse. The transducer is scanned in two directions, collecting waveforms spaced 30 μm apart in the seal direction and 100 μm apart in the transverse direction. The surface of the packaging material is approximately perpendicular to the beam axis, and the sample is kept in the focal region of the transducer throughout the scan. The signal is captured by a digitizing oscilloscope (9354TM; LeCroy, Chestnut Ridge, NY) with a sampling rate of 500 MHz, keeping 512 samples for each transducer position. This data set is also used in [6], and [7] to form BAI images.

III. B-Mode and BAI Images of Channels

B-mode and BAI imaging techniques have been investigated previously to determine their usefulness for detecting channel defects. B-mode images require only a two-dimensional data set rather than a three-dimensional data set. The axis of the channel is oriented perpendicular to the beam axis and also perpendicular to the scanning direction. B-mode images of moderate and small channels are shown in Fig. 1. In these images, the channel orientation is perpendicular to the page. Images in Fig. 1(a and b) are formed using the same data set. Fig. 1(a) shows a B-mode image of a 50-μm (ACP) defect without aligning the received signals. Fig. 1(b and c) shows a 50-μm defect and a 10-μm (ACP) defect, respectively, after the RF signals have been aligned to provide an image that is surface-justified. The justification is accomplished by aligning the signals according to when the pressure reaches its maximum, taking advantage of the fact that the first reflection from the surface of the package has the greatest amplitude.

The appearance of channels in a B-mode image depends on the size of the channel relative to the size of the focal spot of the transducer used. Moderate channels (with diameter between 1/5 and 1 times the lateral dimension of the focal spot) appear as a bright spot at the interface at the top of the channel and a shadow behind the chan-

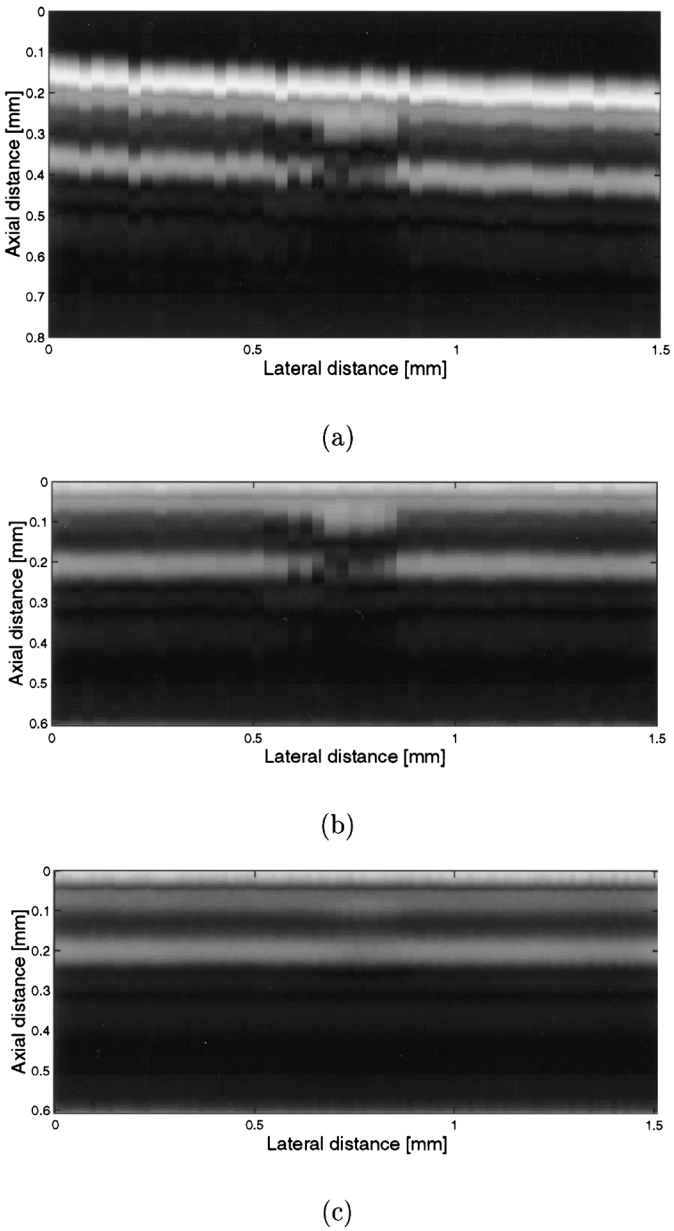

Fig. 1. B-mode images of channels: a) 50-μm ACP trilaminate film before alignment, b) channel from "a" after alignment, c) 10-μm ACP trilaminate film. The larger channel is visible as a brighter region at the top of the channel and a shadow behind the channel. The smaller channel is difficult to see, inspiring the search for a method to produce higher contrast images.

nel. In Fig. 1(a), the backwall reflection appears across the field of view at approximately 0.4 mm in the axial direction. In Fig. 1(b), the backwall reflection appears across the field of view at an axial distance of 0.2 mm. The channel is detected as the bright pixels centered at 0.75 mm in the lateral direction and 0.1 mm in the axial direction and by the shadow at 0.75 mm in the lateral direction and 0.2 mm in the axial direction. Small channels show a slight change in brightness at the location of the channel or they do not appear at all. For example, 15-μm channels have an average change in brightness of 10.3%, for which the percent change is calculated as the change in average pixel brightness divided by the average pixel brightness at the same depth where there is no channel. In Fig. 1(c), the backwall reflection appears across the field of view at an axial distance of 0.2 mm, and the channel is barely observed at a position centered at 0.75 mm in the lateral direction and 0.08 mm in the axial direction.

The BAI technique was introduced to improve the detectability of channel defects. It is a form of C-mode imaging rather than B-mode imaging. BAI images of a 50-μm and a 10-μm ACP trilaminate film are shown in Fig. 2. In these images, the channels lie in the plane of the page. The axis of the defect is perpendicular to the transducer beam axis; however, the transducer is scanned across the defect and along the axis of the defect. BAI images in which a channel is detected have two mean brightness levels, a high value at which there is no channel, and a low value at which the channel exists. Because the maximum and minimum brightness levels define the dynamic range of the image, BAI images of channels can have higher contrast than B-mode images, which include a high brightness level because of the reflection from the front surface as well as a low brightness level from the tail of the received signal.

The BAI technique works well to increase the contrast of moderate-sized channels. By summing the backscattered amplitude, the channels, which manifest themselves as shadows in the back reflection, appear darker than the areas at which there is no channel. However, for small channels, there is little change in the reflection from the back of the material and minor change at the channel location between the layers. Therefore, other changes in the reflected signal, for example those caused by surface roughness, mask the changes in BAI value caused by the presence of the channel, making it difficult to detect channels with a diameter of 15 μm or less. RFS and RFC are expected to improve images of small channels by including only information from the region where the change caused by the presence of the channel is the greatest.

IV. Image Formation

The formation of BAI images has been described previously. The received waveform is envelope-detected using the Hilbert transform, and the resulting envelope is integrated to produce a single BAI value for each position of the transducer. The two-dimensional BAI matrix is then linearly interpolated by a factor of two in the sealing direction and by a factor of seven transverse to the sealing direction, yielding an image pixel size of 15.0 μm by 14.3 μm [4]. This interpolation is also used by the other image formation methods.

A. RFS-Mode Imaging

To create RFS images, the waveforms at each transducer position are first justified in time as shown in Fig. 1. This alignment corrects for flaws in the surface of the pack-

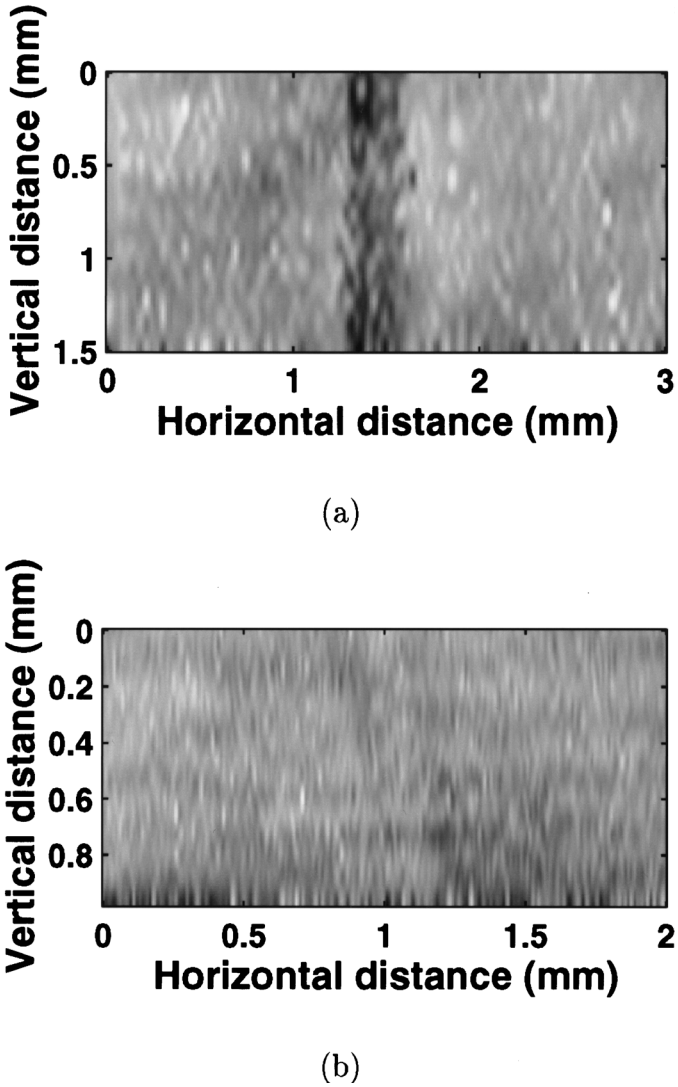

Fig. 2. BAI images of channels: a) 50-μm ACP trilaminate film and b) 10-μm ACP trilaminate film.

age and for the fact that the package surface is not perfectly perpendicular to the beam axis, both of which would change the absolute time to the first reflection for each waveform. For each position of the transducer, a single sample of the time-justified waveform is kept. Because of the sampling process, each sample of the waveform represents an integral of the analog waveform over a 10-ps window. Thus, BAI and RFS images represent two extremes of C-mode imaging, one using the envelope of the entire received waveform and the other using only one sample of the RF waveform.

For RFS to be useful, it must be possible to detect channels of all sizes by creating a few images for each data set. Unfortunately, the time gate that results in the highest contrast image varies with channel size. For channels larger than 15 μm, high contrast images are formed by selecting a time gate close to the temporal location where the backwall reflection would occur when no channel is present. For channels 15 μm and smaller, the highest contrast images are formed by choosing a time gate near the temporal location of the bondline (center) between the two layers. Both time gates are calculated using the measured speed of sound in the packaging material. We do not use the sampling point near the bondline of the package for the large channels because there is more variation in the location where the reflection from the front of the channel will occur. We do not use the sampling point near the backwall for small channels because the difference in signals at and away from channels is often too small to detect in an image.

Within the group of samples for one channel size, there is still some small variation in the time gate that produces the highest contrast image. However, because the primary goal is to detect the channels and producing the best image is secondary, it is possible to choose two appropriate time gates to produce all of the images for all of the channel sizes.

It is possible that time gates chosen based on a priori knowledge of speed of sound and layer thickness will create low contrast images because waveforms received from locations where there is a channel and locations where there is no channel will cross, that is, have similar values at the chosen time gate. This risk of missing a channel defect that is present is the major drawback of choosing a single time gate and was often the case for the aluminum foil films. To reduce the risk, different time gates were chosen experimentally. The aluminum foil films illustrate the difficulty in implementing RFS; however, the difficulty is overcome by choosing proper time gates with a set of calibration data for the material used.

B. RFC-Mode Imaging

To create an RFC image, a reference RF signal is first chosen to represent the RF signal not passing through the channel defect. We assume that there is no channel defect close to the boundary of the scan region, so we take the average of the first five RF signals and regard the averaged signal as the reference signal. Fig. 3 shows an example of two difference signals. The dashed line is an RF signal passing through the channel defect minus the reference signal, and the solid line is an RF signal not passing through the channel defect minus the reference signal. In these plots, the channel defect is 6-μm ACP trilaminate film. It is clear that the difference is relatively large for the RF signal that passes through the channel defect compared with the difference for the signal that does not pass through the channel defect. For the figure, the reference signal is subtracted to show the differences when a channel is present and when it is not; however, for the image formation, we use the correlation coefficient, which does not depend on differences in amplitude.

After forming a reference signal, we next calculate the normalized correlation coefficient between the reference signal and the RF signal at each transducer position to determine the difference between the two ultrasound echoes. Finally, the RFC image is created by displaying the normalized correlation coefficients for each transducer posi-

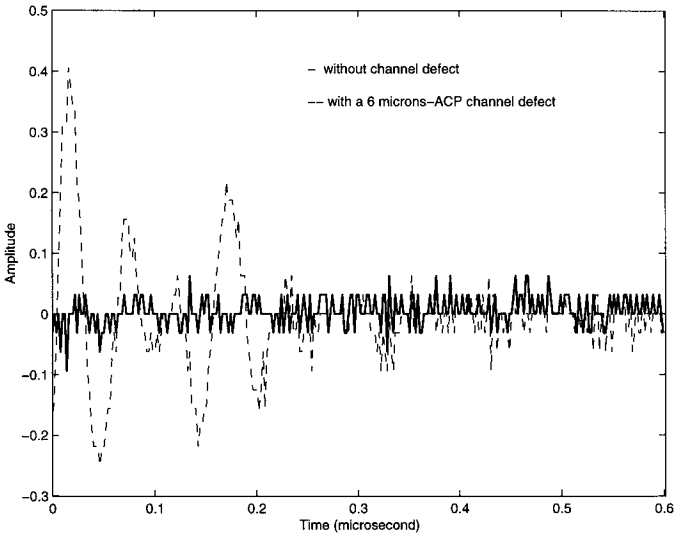

Fig. 3. Difference of RF signals and reference signal in the correlation window.

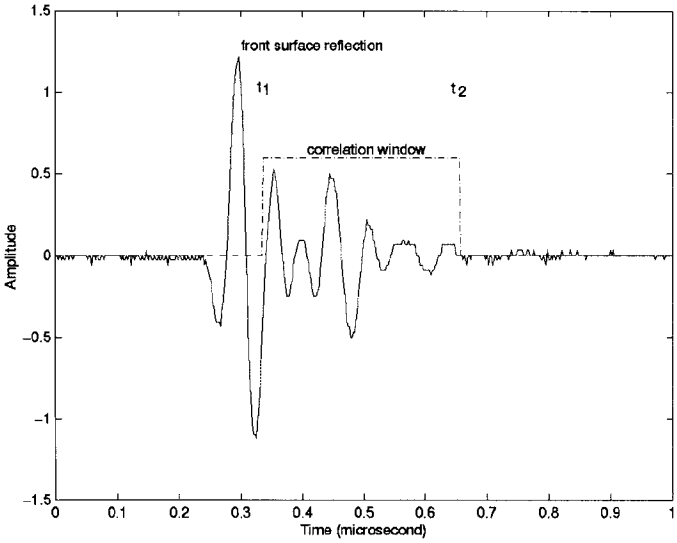

Fig. 4. A 17.3-MHz RF signal with 6-μm ACP trilaminate film.

tion forming a two-dimensional matrix.

To implement this technique, we must choose the window at which the correlation coefficient is calculated. In this work, the following two cases are studied.

- The correlation window is placed covering the entire range of the RF signal starting from the front surface of the package material. The channel defect must be located within the correlation window. This case is denoted as the RFCE.
- The correlation window is placed covering only a short, specified part of the RF signal. In this case, the correlation window is placed between t_1 and t_2 in Fig. 4. There is uncertainty as to whether the channel defect is located within the correlation window; therefore, a coarse estimation of the channel defect range is needed. This case is denoted as RFCS.

C. Performance Measures

The response of an imaging system to a high contrast target is often described by a quantity such as lateral resolution (beamwidth). For targets that have lower echogenicity than the background, such as cysts in medical imaging or channels in the present application, a different quantity is required to summarize the system response. Cyst detectability depends on both beamwidth and sidelobe level because sidelobes have the effect of "filling in" the cyst with reflections from the background when the mainlobe is over the cyst. Cyst detectability also depends on speckle noise.

ΔBAI was the quantity used to describe the contrast of BAI images. It was defined as the difference between the average BAI values of the background and the channel, divided by the maximum BAI value in the image [4]–[7]. In [6], non-normalized ΔBAI values are calculated so that differences between materials can be observed. ΔBAI is useful for BAI images for which the BAI value is always positive; however, it is an awkward measure for RFS and RFC images, in which case pixel values can be positive or negative.

There has been significant consideration in the literature given to quantifying system performance in lesion detection [8]–[10]. The results show that contrast is an important factor for cyst detectability, but CNR, which includes the effect of speckle and noise, is a more complete description of detectability.

Local contrast is defined as $(S_b - S_c)/S_b$, where S_b is the mean value of the background image brightness and S_c is the mean value of the channel [9], [10]. This measure is useful for images that will be logarithmically compressed. We measure the image contrast defined as the mean value of the background minus the mean value of the channel divided by the total range in the image

$$C = \frac{\frac{1}{N_b}\sum_i p_{b_i} - \frac{1}{N_c}\sum_i p_{c_i}}{\max_i p_i - \min_i p_i} \tag{1}$$

where p_i represents an image pixel, N is the total number of pixels, and the subscripts b and c indicate pixels in the background or in the channel, respectively. To define CNR, the noise is defined as the standard deviation of the background pixels, σ_b. CNR is

$$CNR = \frac{C}{\sigma_b}. \tag{2}$$

This CNR is similar to the CNR described by Li and O'Donnell [11]; however, this CNR is applied to images that have not been logarithmically compressed.

In this work, five spatially separated regions covering the background are used to calculate the mean pixel value and the corresponding standard deviation. Three spatially separated locations in the defect region are used to calculate the mean pixel value in the defect.

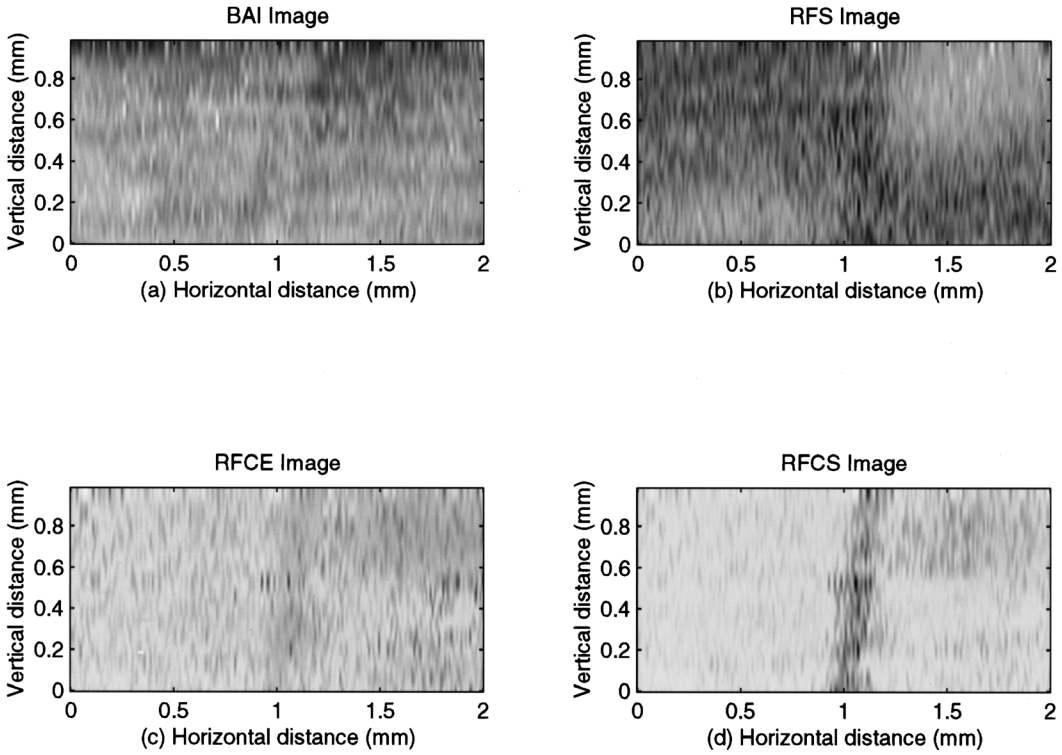

Fig. 5. Processed images for 10-μm, ACP trilaminate film: a) BAI, b) RFS (0.082 μs), c) RFCE, and d) RFCS ($t_1 = 0.08$ and $t_2 = 0.14$, where t_1 and t_2 are given in terms of microseconds after the pressure maximum).

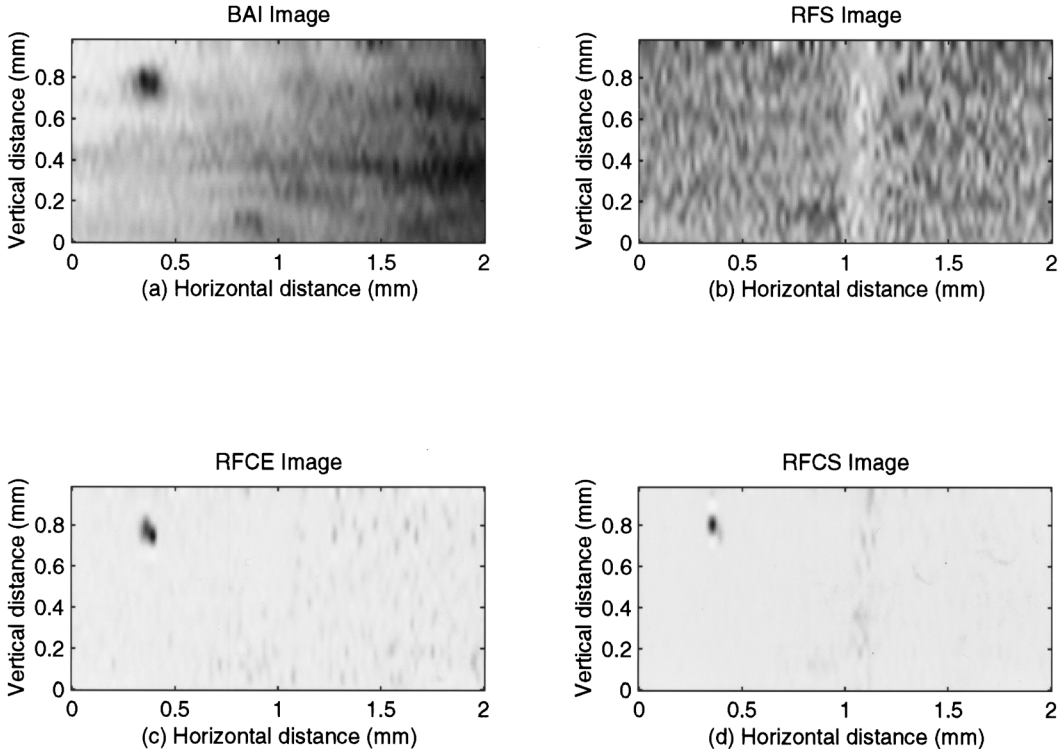

Fig. 6. Processed images for 6-μm, ACP trilaminate film: a) BAI, b) RFS (0.082 μs), c) RFCE, and d) RFCS ($t_1 = 0.08$ and $t_2 = 0.12$, where t_1 and t_2 are given in terms of microseconds after the pressure maximum).

TABLE I
EVALUATION OF ROBUSTNESS BASED ON THE DETECTION RATE.

Film/ channel	Size (μm)	BAI	RFS	RFCE	RFCS
Plastic/ water (WCP)	50	5/5	5/5	5/5	5/5
	38	5/5	5/5	5/5	5/5
	15	2/7	3/7	4/7	5/7
	10	4/5	3/5	2/5	4/5
	6	1/4	3/4	2/4	2/4
Plastic/ air (ACP)	50	5/5	5/5	5/5	5/5
	38	5/5	5/5	5/5	5/5
	15	6/6	6/6	6/6	6/6
	10	3/5	3/5	4/5	5/5
	6	1/4	3/4	2/4	2/4
Foil/ water (WCA)	50	5/5	5/5	5/5	5/5
	38	5/5	5/5	5/5	5/5
	15	3/5	4/5	3/5	5/5
	10	0/6	5/6	1/6	4/6
	6	3/4	4/4	0/4	2/4
Foil/ air (ACA)	50	5/5	5/5	5/5	5/5
	38	5/5	5/5	5/5	5/5
	15	2/8	7/8	4/8	8/8
	10	4/5	4/5	1/5	5/5
	6	4/4	4/4	0/4	4/4

V. RESULTS

Four to eight data sets were collected for each combination of channel size, type of packaging film, and material in the channel. The specific number of samples for each case is apparent in Table I. In this work, we only examine channel sizes 50 μm and smaller because larger defects can be easily detected by any of the previously described imaging techniques.

Fig. 5 and 6 show images created with each technique. In Fig. 5, the defect is a 10-μm ACP trilaminate film. The defect is most easily seen in the image created using RFCS [Fig. 5(d)]. In Fig. 6, the defect is a 6-μm ACP trilaminate film. The defect is detected in the RFS and RFCS images Fig. 6(b and d). The RFS image has greater contrast, but the RFCS image has the smoother background.

Table I shows the detection rates for BAI, RFS, RFCE, and RFCS. All four techniques reveal 100% of channels 38 μm or larger, regardless of the type of channel defect. From this table, we have the following conclusions. 1) BAI imaging performance varies greatly for small channel sizes (i.e., 6, 10, and 15 μm). Although BAI mode imaging allows us to detect some channels as small as 6 μm, we can only detect channels down to 38 μm reliably. 2) The detection rate for RFS imaging technique is comparable with the detection rate for RFCS. The RFS technique is slightly more likely than RFCS to miss a 10- or 15-μm channel and slightly less likely than RFCS to miss a 6-μm channel. Further testing with a larger number of samples would be necessary to determine whether the differences in detection rates for these two techniques are significant. 3) RFC is not sensitive to correlation range for the larger channel defects, i.e., 38 and 50 μm. Both RFCE and RFCS achieve 100% detection. 4) RFC is very sensitive to the correlation range for the small channel, i.e., smaller than 15 μm. The smaller the channel size, the more sensitive RFC is. For example, RFCS still achieves 50 and 100% detection of channel size 6 μm for WCA and ACA, and RFCE has 0% detection for these same channel defects. Therefore, the appropriate choice of correlation window plays an important role in RFC.

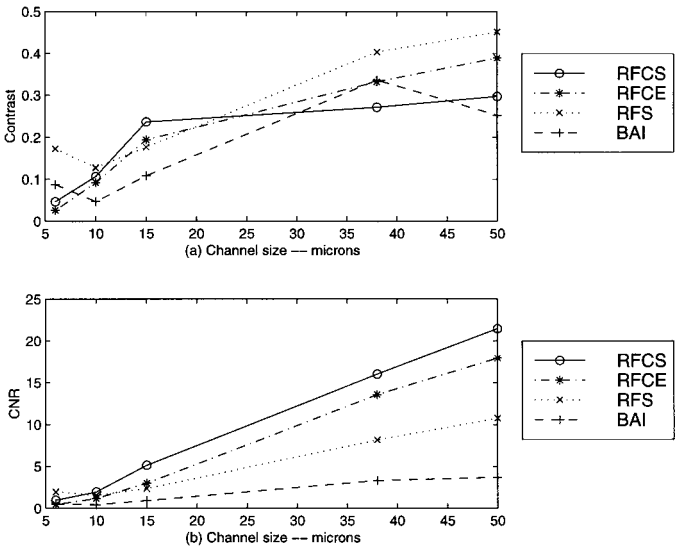

Fig. 7. a) Contrast and b) CNR for ACP trilaminate film.

The contrast versus channel size for ACP trilaminate film is shown in Fig. 7(a). BAI has the lowest contrast for 10- and 15-μm channels. RFS achieves the highest contrast enhancement among all four imaging techniques for all channels except 15 μm. Contrast, a dimensionless quantity, is approximately 0.05 larger for 38- and 50-μm channels. CNR versus channel size for ACP trilaminate film is shown in Fig. 7(b). Clearly, RFCS and RFCE have sharper curves than RFS and BAI. CNR separation becomes larger as channel size increases, demonstrating that RFC technique has the better capability to smooth the background than the other techniques. This property is an advantage of RFC technique over RFS and BAI. Similar results are obtained for WCP trilaminate film (not shown.)

Fig. 8 shows the contrast and CNR versus channel size for WCA foil containing film. The RFS method shows larger contrast than all other methods for channels 15 μm and smaller and larger contrasts than RFCE and RFCS, respectively, for 38-μm channels. Although RFCS is not the best in terms of contrast enhancement, it has by far the greatest CNR enhancement. Once more, it shows the capability of RFCS to smooth the background area, i.e., smallest standard deviation of the background contrast. Similar results are obtained for ACA foil film (not shown).

The success of the RFS imaging method in detecting channels is related to the high degree of uniformity of the sample thickness. The samples were examined for their uniformity by looking at the received signals after the image formation had been completed. After justifying all of

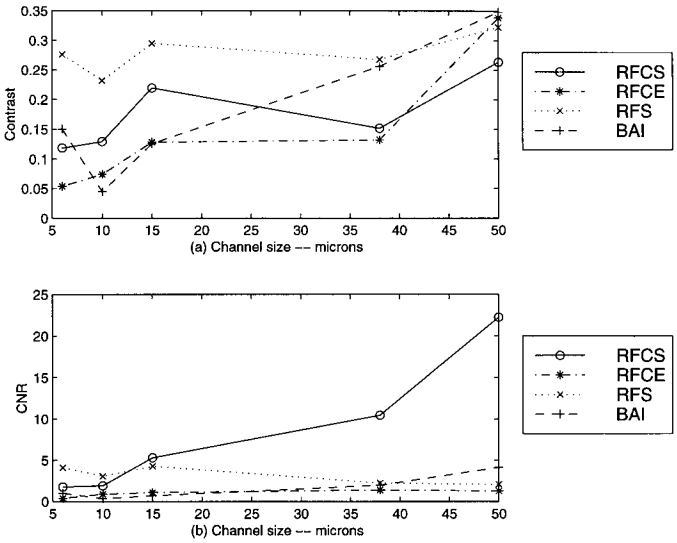

Fig. 8. a) Contrast and b) CNR for WCA.

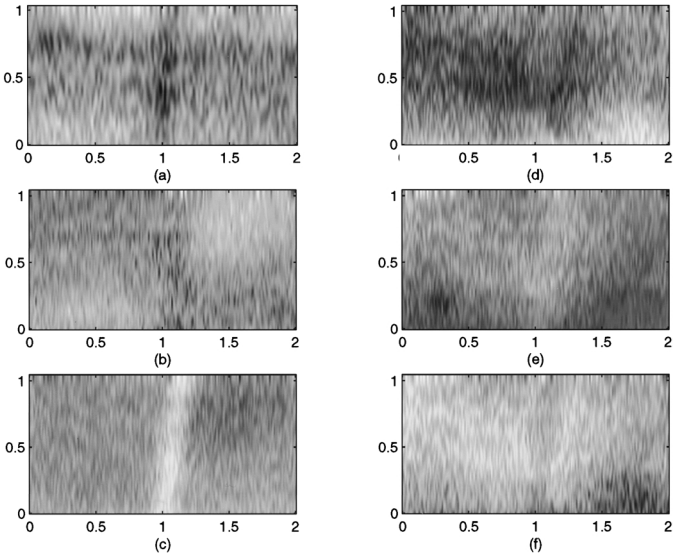

Fig. 9. Example of how RFS could be used in a production line. Six RFS images are shown for the same data (10-μm ACP trilaminate film) using time gates a) 0.082, b) 0.092, c) 0.102, d) 0.174, e) 0.184, and f) 0.194. Time gates are expressed in microseconds and are measured from time of the peak acoustic pressure.

the signals, the time elapsed from the pressure maximum (the peak pressure from the reflection at the front surface) to the peak pressure from the reflection at the back surface was measured for each waveform. For the plastic trilaminate film, we found that the time to the maximum acoustic pressure from the back reflection ranged from 0.156 to 0.160 μs for all channel sizes. For the aluminum foil film, there was much more variation. The mean time of the peak of the back reflection, averaged for each channel size and filling material varied from 0.182 to 0.217 μs. Within one package sample, the variance was as high as 0.018 μs. This variability means that it is difficult to pick a single time gate to detect all channels. Hence, RFS would be more difficult to use for materials with a high variation in thickness.

RFS allows us to create high contrast images very quickly; however, because of the oscillations of the carrier signal, it can be difficult to find the location of the time gate that will produce a high contrast image for every defect. Therefore, channels will go undetected more often. To increase the reliability for use on a production line further, multiple images of the same package should be created. This method of operation is still practical because no computation is required to form the images, and, therefore, multiple images can be generated quickly. An example of how this technique could be used in a production line is shown in Fig. 9. The figure shows images of the 10-μm diameter channel of Fig. 5. Three time gates close to the bondline and three close to the backwall are shown because we do not assume a priori knowledge of channel size. In this case, the channel is clearly revealed in Fig. 9(c). It can also be detected in Fig. 9(a) and possibly in Fig. 9(f).

RFCS uses more information from the received signal and, therefore, does not suffer as much as RFS with the variability in the package, nor does it require the formation of several images per package.

VI. Conclusions and Future Work

In this paper, three imaging techniques are compared on the basis of detection rate, image contrast, and CNR to evaluate their performance in detecting channel defects. We have shown that RFS and RFCS are superior to the current BAI method for reliably detecting channel defects less than 38 μm in diameter. Overall, the techniques that limited the information to that closest to the defect performed the best, as might be expected.

With RFS, we are able to detect channels as small as 6 μm in diameter using pulse-echo ultrasound with a 17.3-MHz transducer. This imaging method has been applied to a special imaging problem for which we have significant information about the material properties and the location of the channel defect. Given this a priori knowledge, we are able to select two time gates to create images. The plastic trilaminate film is an example of a material to which RFS can be applied with ease. The aluminum foil trilaminate film, for which sound speed and layer thickness are less uniform is an example of a material to which the RFS technique is applied with more difficulty.

It was experimentally found that RFC in a short, specified window generally has the highest detection rate and greatest CNR enhancement. Also, because the correlation is done within a short, specified range, RFCS is more computationally efficient than the traditional BAI for which the integral of the envelope-detected RF signal is over the entire RF signal range. And, unlike the RFS technique, RFCS can be used as easily with either of the two layered materials.

Based on the results from the RFC study, we modify the traditional BAI technique and integrate only over the specified range used for RFCS. The results we have so far

are promising and show the improvement in detection rate and CNR enhancement. Further investigation is needed. Future work also includes finding a way to choose the optimal correlation window automatically for RFC, using image segmentation algorithms to detect channels automatically and collecting data on a larger number of samples for a complete statistical study.

Acknowledgment

The authors gratefully acknowlege the professional assistance with the sample validations by James F. Zachary, DVM, Ph.D., Department of Veterinary Pathobiology, University of Illinois.

References

[1] C. L. Harper, B. S. Blaikistone, J. B. Litchfield, and S. A. Morris, "Developments in food package integrity testing," *Food Technol.*, vol. 6, no. 10, pp. 336–340, 1995.

[2] B. G. Frock and R. W. Martin, "Applications of digital image enhancement techniques to the ultrasonic NDE of composite materials," *Acoust. Imaging*, vol. 15, pp. 461–469, 1987.

[3] R. Kazys and L. Svilainis, "Ultrasonic detection and characterization of delaminations in thin composite plates using signal processing techniques," *Ultrasonics*, vol. 35, no. 5, pp. 367–383, 1997.

[4] K. Raum, A. Ozguler, S. A. Morris, and W. D. O'Brien, Jr., "Channel defect detection in food packages using integrated backscatter ultrasound imaging," *IEEE Trans. Ultrason., Ferroelect., Freq. Contr.*, vol. 45, no. 1, pp. 30–40, Jan. 1998.

[5] A. Ozguler, S. A. Morris, and W. D. O'Brien, Jr., "Evaluation of defects in seal region of food packages using the backscattered amplitude integral (BAI) technique," in *1997 IEEE Int. Ultrason. Symp.*, Toronto, ON, Canada, pp. 689–692.

[6] ——, "Evaluation of defects in seal region of food packages using the ultrasonic contrast descriptor, ΔBAI," *Packaging Technol. Sci.*, vol. 12, no. 4, pp. 161–171, 1999.

[7] ——, "Ultrasonic imaging of micro-leaks and product contamination in flexible food packages by pulse-echo technique," *J. Food Sci.*, vol. 63, no. 4, pp. 673–678, 1998.

[8] S. W. Smith, R. F. Wagner, J. M. Sandrik, and H. Lopez, "Low contrast detectability and contrast/detail analysis in medical ultrasound," *IEEE Trans. Sonics Ultrason.*, vol. 30, no. 3, pp. 164–173, May 1983.

[9] D. H. Turnball, P. K. Lum, A. T. Kerr, and F. S. Foster, "Simulation of B-scan images from two-dimensional transducer arrays: Part I – Methods and quantitative contrast measurements," *Ultrason. Imag.*, vol. 14, no. 4, pp. 323–343, 1992.

[10] S.H.P. Bly, D. Lee-Chahal, D. R. Foster, M. S. Patterson, F. S. Foster, and J. W. Hunt, "Quantitative contrast measurements in B-mode images comparison between experiment and theory," *Ultrason. Med. Biol.*, vol. 12, no. 3, pp. 197–208, 1986.

[11] P.-C. Li and M. O'Donnell, "Improved detectability with blocked element compensation," *Ultrason. Imag.*, vol. 16, no. 1, pp. 1–18, 1994.

Catherine (Kate) Frazier (S'92) was born on August 16, 1972 in Bethesda, MD. She received the B.S.E.E. from the University of Maryland at College Park in 1994 and the M.S. in Electrical Engineering from the University of Illinois at Urbana-Champaign in 1996. For her M.S. thesis, she investigated the use of a virtual source in synthetic aperture imaging algorithms. She received the Ph.D. in Electrical Engineering from the University of Illinois in 2000. For her dissertation, she developed signal processing algorithms for and simulated the operation of a two-dimensional amplitude-steered array for real-time volumetric imaging.

Ms. Frazier was awarded the National Science Foundation Fellowship from 1994 to 1997 and the Koehler Fellowship for the 1994–1995 academic year. In April 1997, she was presented the Robert T. Chien Memorial Award for outstanding research in electrical engineering. She received a Selected Professions Fellowship from the American Association of University Women in July 1999.

Her research interests are in acoustical image formation and signal processing. The applications have included nondestructive evaluation of defects in package seals, subsurface imaging, and a diver-held sonar camera.

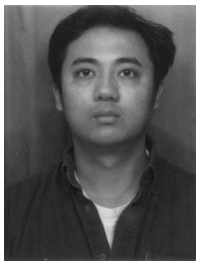

Qi Tian (S'95–M'96) was born in Chengdu, China on January 19, 1970. He received the B.E. degree in Electronic Engineering from Tsinghua University, P. R. China, in July 1992 and M.S. degree in Electrical Engineering from Drexel University, Philadelphia, PA, in June 1996. He is currently pursuing the Ph.D. degree in Electrical and Computer Engineering at the University of Illinois at Urbana-Champaign. He was a graduate research and teaching assistant in the Department of Electrical and Computer Engineering at Drexel University from 1994 to 1997 and a graduate research assistant in the Bioaccoustics Research Laboratory of the Beckman Institute for Advanced Science and Technology at UIUC from August 1997 to January 1999. Since February 1999, he has been a graduate research assistant at the Image Formation and Processing Group of the Beckman Institute for Advanced Science and Technology at UIUC.

His current research interests include multimedia content analysis and retrieval, digital image and signal processing, computer vision, and ultrasonic imaging. He has published over 15 journal and conference papers.

Ayhan Ozguler received B.Sc. degree in Food Engineering from Middle East Technical University, Ankara, Turkey, in 1991 and M.S. and Ph.D. degrees in Food Processing and Engineering from the University of Illinois, Urbana-Champaign, in 1995 and 1999, respectively.

From 1995 to 1999, he was a research assistant at the University of Illinois and was involved in a joint research project between the Packaging Laboratory and the Beckman Bioacoustic Research Laboratory. His main research interests include nondestructive inspection techniques of food packages for the seal integrity and the ultrasonic imaging. Dr. Ozguler is currently employed as a postdoctoral research associate, and his responsibilities include quantifying the engineering trade-offs of using nondestructive ultrasonic sensor and defining the design parameters necessary for the safe, high speed production of shelf-stable foods in new energy- and material-efficient packages.

In 1993, he was awarded the scholarship of Republic of Turkey, Ministry of National Education to pursue master and Ph.D. degrees in the area of food packaging in the U.S. In 1998, he received the reward from the Packaging Education Forum for his contribution

to the field of packaging. Dr. Ozguler is the member of Institute of Food Technologists (IFT) Food Packaging Division and Gamma Sigma Delta.

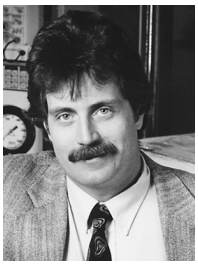

Scott A. Morris received the B.S., M.S., and Ph.D. degrees in 1981, 1987, and 1992 from Michigan State University.

While employed at Michigan State University, he worked with a variety of problems related to the packaging industry. Development of an experimental permeation modeling technique utilizing a combination of numerical modelling, optical measurement techniques, and laboratory analytical testing methods. Microwave cooking of frozen and shelf-stable foods, and the redesign of their related package systems. Improved shipping designs for retortable-pouch packaging systems. Development of chromatographic methods for the evaluation of volatile extractables from packaging materials. Determination of oxygen-barrier requirements of products that had been previously packaged in impermeable cans, and the evaluation of the suitability of producer-supplied polymeric replacements. Development of a research program in conjuction with a major packaging corporation, to test the ability of their 2-liter aseptic package to survive shipping and distribution. A survey of the state-of-the-art of packaging in the United States, and significant trends in the technical and economic aspects of the packaging industry commissioned by the Congressional Office of Technical Assessment (OTA). Investigating the relationship of package design to the effects of shock, vibration and compression on fresh and controlled-atmosphere-stored produces gaseous metabolic by-products.

Now an Associate Professor, Dr. Morris has been at the University of Illinois Departments of Food Science and Human Nutrition and Agricultural Engineering since 1992. He currently is developing a packaging research and teaching program. Current research projects within the program include: leak detection in shelf-stable food packages using high-frequency ultrasound, predictive modeling of package-structure permeation properties; static and dynamic structural modeling for design strength, and material-use optimization; packaging line efficiency optimization; product quality degradation from mechanical input and thermal variation; time-dependent material properties from stress-strain histories using recursive finite element algorithms; and microwave energy dispersion in food packages.

Dr. Morris is a member of the executive committee of the Institute of Food Technologists (IFT) Food Packaging Division, a member of the American Society of Agricultural Engineers (ASAE), Society of Professional Engineers (SPE), Institute of Packaging Professionals (IoPP), American Society for Engineering Education (ASEE), Pi Kappa Gamma, and Gamma Sigma Delta.

William D. O'Brien, Jr. (S'64–M'70–SM'79–F'89) received the B.S., M.S., and Ph.D. degrees in 1966, 1968, 1970, from the University of Illinois, Urbana-Champaign.

From 1971 to 1975 he worked with the Bureau of Radiological Health (currently the Center for Devices and Radiological Health) of the U.S. Food and Drug Administration. Since 1975, he has been at the University of Illinois, where he is a Professor of Electrical and Computer Engineering, and Professor of Bioengineering, College of Engineering and of Bioengineering, College of Medicine. He is the Director of the Bioacoustics Research Laboratory and the Program Director of the NIH Radiation Biophysics and Bioengineering in Oncology Training Program. His research interests involve the many areas of acoustics and ultrasound, including spectroscopy, risk-assessment, biological effects, tissue characterization, dosimetry, blood-flow measurements, acoustic microscopy, and imaging. He has published more than 180 papers.

Dr. O'Brien is Editor-in-Chief of the *IEEE Transactions on Ultrasonics, Ferroelectrics, and Frequency Control.* He is a Fellow of the Institute of Electrical and Electronics Engineers (IEEE), the Acoustical Society of American (ASA), and the American Institute of Ultrasound in Medicine (AIUM), and he is a Founding Fellow of American Institute of Medical and Biological Engineering. He was recipient of the IEEE Centennial Medal (1984), the AIUM Presidential Recognition Awards (1985 and 1992), the AIUM/WFUMB Pioneer Awards (1988), the IEEE Outstanding Student Branch Counselor Award (1989), and the AIUM Joseph H. Holmes Basic Science Pioneer Awards (1993). He has been President (1982–1983) of the IEEE Sonics and Ultrasonics Group (currently the IEEE UFFC Society), Co-Chairman of the 1981 IEEE Ultrasonic Symposium, President of the AIUM (1988–1991), and Treasurer of the World Federation for Ultrasound in Medicine and Biology (1991–1994). He is the 1997–1998 IEEE UFFC Society's Distinguished Lecturer.